

# SILICON NANOSTRUCTURES FOR PHOTONICS

L. Pavesi, P. Bettotti, M. Cazzanelli, S. Cella, N. Daldosso, L. Dal Negro, B. Danese, Z. Gaburro,  
C. J. Oton, L. Pancheri, G. Vijaya Prakash  
INFN and Dipartimento di Fisica, Università di Trento  
via Sommarive 14, 38050 Povo Trento

**Abstract** Nanostructuring silicon is an effective way to turn silicon into a photonic material. In fact low dimensional silicon shows light amplification characteristics, non-linear optical effects, photon confinement in both one and two dimensions, photon trapping with evidences of light localization, and gas sensing properties.

**1. Introduction** Silicon (Si) is the leading material concerning high-density electronic functionality. Integration and economy of scale are the two key ingredients for the technological success of Si. Its band-gap (1.12 eV) is ideal for room temperature operation, and its oxide (SiO<sub>2</sub>) allows a processing flexibility to place more than 10<sup>8</sup> transistors on a single chip. However all the single transistors and electronic devices have to transfer information on length scale which are relevant with respect to their nanometer scale. Lengths of 15 Km in a single chip are today common, while in ten years these will reach more than 91 Km [1]. This interconnection degree is sufficient to cause relevant propagation delays, overheating, and information latency. Overcoming this interconnection bottleneck is one of the main motivation and opportunity for the present-day Si-based microphotonic [2]. Microphotonic attempts to combine photonic and electronic components on a single Si chip. Both hybrid and monolithic approaches are possible. Replacement of electrical with optical interconnects has appealing potentialities, such as high speed performance and immunity to signal cross talk.

The development of Si-based photonics has been far behind the development of electronics for long time. The main reason of such slow progress has been the lack of practical Si light sources, i.e., efficient Si light emitting diodes (LED) and injection lasers. Si is an indirect band-gap material. Light emission in indirect materials is naturally a phonon-mediated proc-

ess with low probability (spontaneous recombination lifetimes in the millisecond range). In standard bulk Si, competitive non-radiative recombination rates are much higher than the radiative ones and most of the excited e-h pairs recombine non-radiatively. This yields very low internal quantum efficiency ( $\eta_i \approx 10^{-6}$ ) for Si luminescence. As what concerns the lasing of Si, fast non-radiative processes such as Auger or free carrier absorption severely prevent population inversion at the high pumping rates needed to achieve optical amplification. However, during the last ten years, many different strategies have been employed to overcome these material limitations. Present-day Si LEDs are only a factor of ten out of the market requirements [3,4] and optical gain has been demonstrated [5].

Availability of Si nanotechnology had a primary role in these achievements. Today we know that in Si nanocrystals (Si-nc) the electronic states – as compared to bulk Si – are dramatically influenced both by quantum confinement (QC) and by the enhanced role of states – and defects – at the surface. The effect of QC is a rearrangement of the density of electronic states in energy as direct consequence of volume shrinking in one, two or even three dimensions, which can be obtained, respectively, in quantum wells, wires and dots. On the other hand, the arrangement of the atomic bonds at the surface also strongly affects the energy distribution of electronic states, since in Si-nc the Si atoms are either at the surface or few lattice sites away. The QC and a suitable arrangement of interfacial atomic bonds can provide in Si-nc radiative recombination efficiencies that are orders of magnitude larger than in bulk Si, significant optical non-linearity and, even, optical gain [5]. The aim of this work is to review our recent accomplishments in the field of silicon photonics.

**2. Nonlinear optical properties of Si-nc** Besides the linear optical properties, nonlinear optical properties are of major interest for photonics device applications such as all-optical switching. Intensity dependent changes in the optical properties are prominent at high intensities ( $I$ ) of pump laser, particularly third-order nonlinear effects. Enhanced optical nonlinearity has been reported for porous silicon (PS) at different wavelengths [6,7]. Very few reports are available on other kinds of Si-nc [8-10].

Third order nonlinear effects are generally characterized by nonlinear absorption ( $\beta$ ) and nonlinear refractive index ( $n_2$ ). These are described by  $\alpha(I) = \alpha_0 + \beta I$  and  $n(I) = n_0 + n_2(I)$  where  $\alpha_0$  and  $n_0$  stands for linear absorption and refractive index, respectively. The  $\beta$  and  $n_2$  values are used to evaluate the imaginary ( $\text{Im } \chi^{(3)}$ ) and real ( $\text{Re } \chi^{(3)}$ ) parts of the third order nonlinear susceptibility. One of the most versatile technique to measure  $\text{Im } \chi^{(3)}$  and  $\text{Re } \chi^{(3)}$  is the single beam technique, referred as z-scan [11,12]. The measure of the transmission (with and without an aperture in the far field) as the sample moves through the focal point of a lens ( $z$  axis), enables the separation of the nonlinear refractive index from the nonlinear absorption. For all the investigated samples, the closed aperture data show a distinct valley-peak configuration typical of positive nonlinear effects (self focusing), as expected for most of dispersive materials [13]. From a fit of the z-scan curve,  $n_2$  is obtained. The real part of the third-order nonlinear susceptibility is obtained from  $\text{Re } \chi^{(3)} = 2n_0^2 \epsilon_0 c n_2$ , where  $\epsilon_0$  is the permittivity of free space and  $c$  is the velocity of light. The effective refractive index,  $n_0$  is considered to be 1.7, obtained from independent measurements on these samples. For the measurements shown in Figure 1 (top plot),  $\text{Re } \chi^{(3)} = (1.3 \pm 0.2) \times 10^{-9}$  esu.

Fig. 1B shows the normalized open aperture transmission (full power into the detector) as a function of  $z$ . When direct absorption is negligible, one can deduce  $\beta$ , from the open aperture z-scan data.

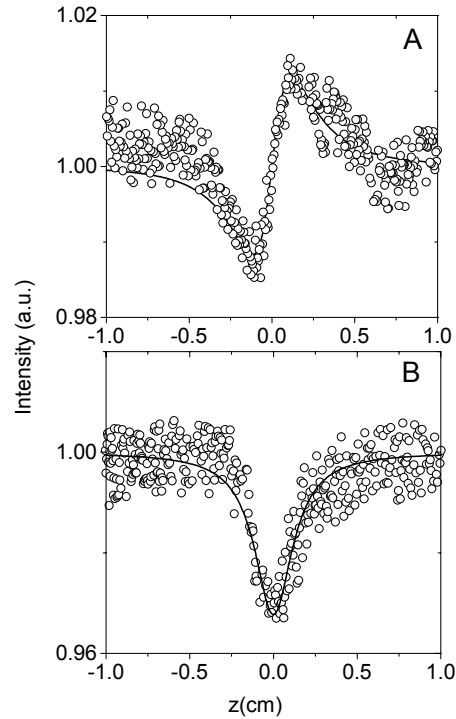


Figure 1. (A) Closed aperture Z scan for Si-nc ( $\lambda = 800\text{nm}$ , pulse width =60 fs). (B) Open aperture Z scan.

The open aperture experiment is done for repeated times and for different peak intensities between  $0.3$  to  $2 \times 10^{10} \text{W/cm}^2$  to ensure proper measurements. The measured  $\beta$  values for Si-nc are higher than the value of crystalline silicon (c-Si) [14] and close to the values for PS. [7] Knowing  $\beta$ , the imaginary part of the third-order nonlinear susceptibility  $\chi^{(3)}$  is evaluated to be  $(0.6 \pm 0.09) \times 10^{-10}$  esu. The nonlinear absorption arises from either direct multiphoton absorption or saturation of single photon absorption. z-scan traces with no aperture are expected to be symmetric with respect to the focus ( $z=0$ ) where they have the minimum transmittance, for two or multi-photon absorption, or maximum transmittance, for saturation of absorption. Fig. 1B shows a well-defined bell shaped minimum transmittance at the focus. All these features are suggesting two-photon absorption (TPA) as the origin of the nonlinear absorption.

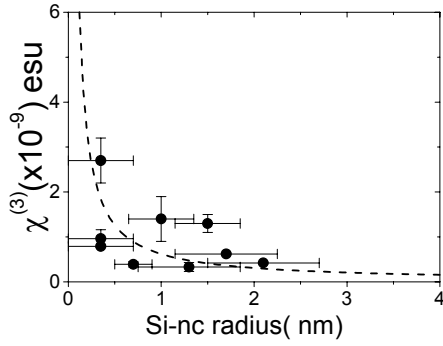


Figure 2. Variation of  $\chi^{(3)}$  with Si-nc radius ( $r$ ) in Si-nc grown by PECVD. Inset shows the PL peak maxima variation with Si-nc radius. Dashed lines are a theoretical fit.

By comparing  $\text{Re}\chi^{(3)}$  and  $\text{Im}\chi^{(3)}$  one can conclude that  $\text{Re}\chi^{(3)} \gg \text{Im}\chi^{(3)}$ , that is the nonlinearity is mostly refractive. The absolute values of  $\chi^{(3)} = ((\text{Re}\chi^{(3)})^2 + (\text{Im}\chi^{(3)})^2)^{1/2}$  are significantly larger than the bulk Si values ( $\sim 6 \times 10^{-12}$  esu) and are of the same orders of magnitude as those reported for PS and for glasses containing nanocrystallites. Quantum confinement effects on  $\chi^{(3)}$  have been estimated in several works [15-17] It was found that the increase in the oscillator strengths caused by the confinement-induced localization of excitons originates the increase of  $\chi^{(3)}$ . The dependence of  $\chi^{(3)}$  on Si-nc radius ( $r$ ) is plotted in Fig. 2. The increase in  $\chi^{(3)}$  is not as sharp as expected by the theoretical model, but follows more closely

$\chi_{\text{Si-nc}}^{(3)} = \chi_{\text{bulk}}^{(3)} + \frac{A}{r} + \frac{B}{r^2}$ . A similar polynomial dependence is theoretically expected for the size dependence of the emission energies of Si-nc [18]. In reality, the experimentally determined  $\chi^{(3)}$  is related to the microscopic  $\chi_m^{(3)}$  by  $\chi^{(3)} = p|f|^4 \chi_m^{(3)}$ , where  $p$  is the volume fraction and  $f$  is a local field correction that depends on the dielectric constant of embedded matrix and nanocrystals. Hence, in addition to  $r$  other parameters such as effective refractive index and volume fraction of Si-nc in the embedded matrix are to be taken into account. This could explain the scatter in the data of Fig. 2.

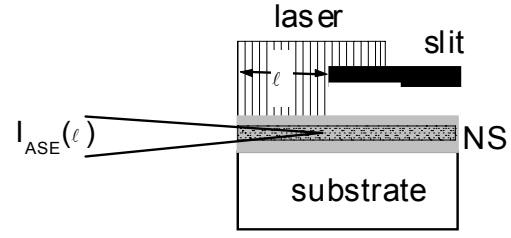


Figure 3. Sketch of the variable stripe length method. The amplified luminescence intensity from the sample edge is recorded as a function of the slit width  $\ell$ .

**3. Optical gain in Si-nc** We have reported single pass gain in pump and probe transmission experiments in ion implanted Si-nc into quartz substrates. [53] We claim that population inversion is possible between the fundamental and radiative Si=O interface states. We found that critical issues to obtain sizeable gain are 1) high oxide quality, 2) high areal density of Si nanocrystals, and 3) proper waveguide geometry of the Si-nc samples. A critical balance between gain and Auger recombination is always present which can prevent gain observation [19]. Other papers confirmed our observations [20-22].

The gain coefficient was measured by the variable strip length method (V.S.L.) where the amplified spontaneous emission intensity, emitted from the sample edge is collected as a function of a linear excitation volume [23]. The V.S.L. method is based on the measure of the luminescence emitted from the sample edge as a function of the linear dimensions of the excited region ( $\ell$ , see Fig. 3). A fit to the resulting curve yields the optical gain  $g$  at every wavelength.

By assuming a one-dimensional amplifier model,  $I_{\text{ASE}}$  can be related to  $g$  by:

$$I_{\text{ASE}}(\ell) \propto \frac{I_{\text{SPONT}}}{g - \alpha} \left( e^{(g - \alpha)\ell} - 1 \right) \quad (3)$$

where  $I_{\text{SPONT}}$  is the spontaneous emission intensity and  $\alpha$  an overall loss coefficient. The gain measured in this way is the modal gain: the material gain weighted by the optical confinement factor of the guided mode.

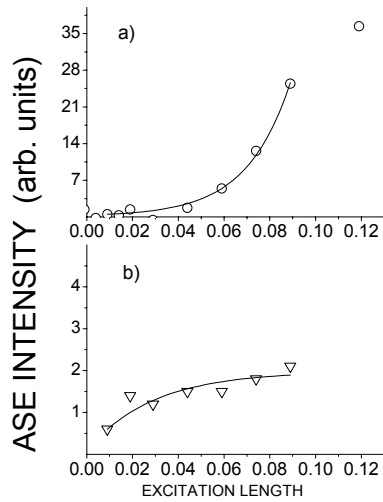


Figure 4. Room temperature VSL curves. The symbols are the data while the lines are the fits. a) VSL at 760 nm at a pumping intensities of  $3\text{ kW/cm}^2$ . The net modal gain coefficient is  $52 \pm 5\text{ cm}^{-1}$ . b) Low power VSL curve at 760nm ( $0.05\text{ kW/cm}^2$ ). The fit yields optical losses of  $34 \pm 5\text{ cm}^{-1}$ .

In Fig. 4, some recent V.S.L. results obtained with high intensity visible excitation on a Si-nc transparent sample are shown. The  $\ell$  range shown in Fig. 4 is the region where the laser excitation has a homogeneous intensity profile and where the light coupling with the physical edge of the sample is free from diffraction artifacts.

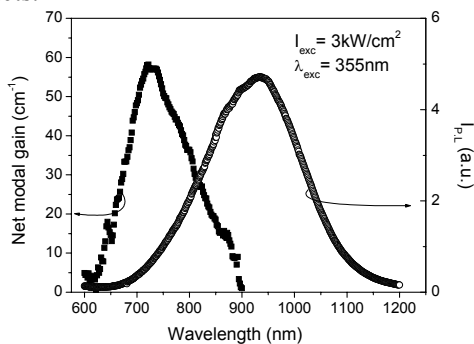


Figure 5. Modal gain spectrum (filled squares) and luminescence spectrum (empty circles) for a nc-Si sample.

To build a model to understand the gain data, we considered that: a) no significant absorption at the luminescence/gain spectral region is observed, b) a great amount of evidences are suggesting that the 750-800 nm near infrared emission band is due to radiative Si=O interface states, c) fast component in the recombi-

nation dynamics appears for high pumping rate (see fig. 6). From these data, a four-level model naturally comes out to explain the gain. Several papers report on the existence of interface states in Si nanocrystals which can trap electrons, and recently more sophisticated models appeared like the Si-Si dimer<sup>4</sup>, the silanone formation and the self trapped exciton [24-28]. The localized nature of the inverted state prevents a significant role of free carriers absorption, because carriers in these states are no longer free but confined. The four-levels could be due to the conduction and valence Si-nc states and an internal transition of the interface states. Indeed the details of the gain model are still under debate. Here what we want to stress is the critical role played by the interface states.

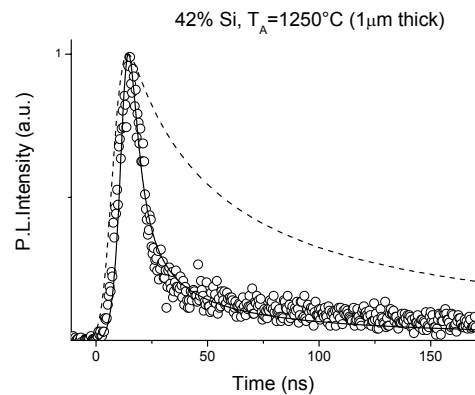


Figure 6 (symbols) Room temperature time resolved decay curve on a  $1\text{ }\mu\text{m}$  thick sample. The detection wavelength was 750nm. (full line) Emitted photon numbers obtained by solving the four levels model with an Auger lifetime of 30 ns, a gain cross section of  $1.2 \times 10^{-17}\text{ cm}^2$ , a Si-nc density of  $6 \times 10^{18}\text{ cm}^{-3}$  and a pumping photon flux of  $10^{19}\text{ photons/(s cm}^2)$ . (dashed line) Emitted photon numbers obtained by solving the four levels model with the same parameters and neglecting stimulated emission. All the curves are normalized to unity.

A four level rate equation which includes both the stimulated transition and the Auger recombination, can reproduce qualitatively the experimental data as shown in Fig. 6. The critical issue for these observations is the critical balance between Auger and stimulated emission.

**4. Porous Si Sensors** The sponge structure of PS is the cause of the high surface/volume ratio, which is typically of the order of  $500\text{ m}^2/\text{cm}^3$ . This is responsible for the high reac-

tivity of PS layers in contact with chemical species. This feature is an advantage if PS is exploited as a sensing material [29]. The sensing activity of PS ranges from  $\text{NO}_2$  [30,31], to humidity [32,33], to organic molecules [29], to ethanol [34], etc. In addition, PS microcavities have been used as biosensor because of their response to DNA molecules and lipids [35], which allows distinguishing viral genetic chains and gram-negative bacteria. Therefore the fields of application of PS sensors are very assorted.

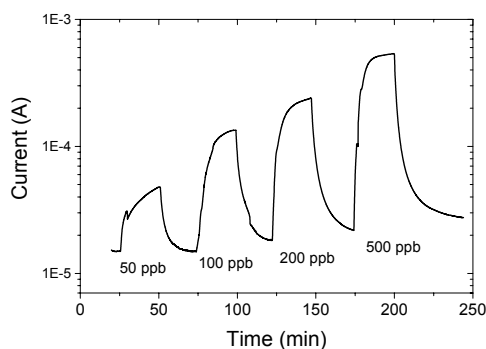


Figure 7. Total current with a bias voltage of 100mV applied between one electrode and the substrate of the 30  $\mu\text{m}$  PS layer. The plot shows the response to the intermittent exposure to different  $\text{NO}_2$  concentrations in dry air.

Different substances affect different physical properties [29]. This can be exploited to distinguish the substances parametrically. One of these sensitive properties is the electrical conductance between two electrodes on the surface of the PS layer. In Fig. 7 it is shown the response of PS in contact with air with very low concentration of  $\text{NO}_2$ . Record level of  $\text{NO}_2$  of 20 ppb can be detected with PS. Also photoluminescence depends sensitively on the surrounding gases. Polar molecules inside the structure quench the luminescence because the electric field created inside the pores due to the dipolar moment of the gas breaks the exciton. This fact allows measuring concentration of polar species taking the integrated PL as the sensing parameter. Another physical parameter, which varies in presence of different gases, is the effective refractive index  $n$  of PS. As the PL peak position ( $\lambda_c$ ) of a microcavity [36] depends on  $n$  as  $\lambda_c = nd$ , where  $d$  is the thickness of the central layer.  $\lambda_c$  is particularly dependent

on the ambient in which the microcavity is immersed. The narrowing of the PL peak in a microcavity allows the measure of small variation of  $n$ , i. e. the detection of low gas concentration.

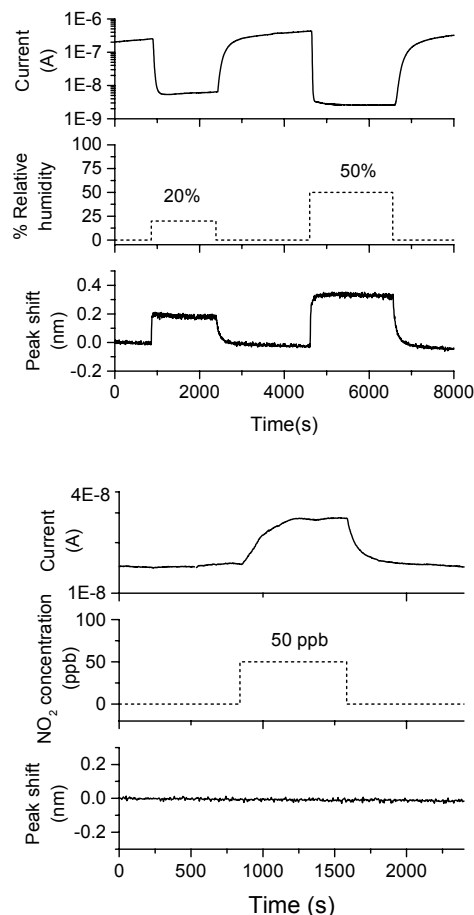


Figure 8. Simultaneous measurement of optical and electrical response to humidity and  $\text{NO}_2$ . The electrical current is measured on the 30  $\mu\text{m}$  deep monolayer employing the three-terminal configuration, and the reflectance peak shift is measured on the microcavity. Left plot: response to two different humidity values in absence of  $\text{NO}_2$ . Right plot: response to 50 ppb of  $\text{NO}_2$  in presence of 20% humid air.

For what above discussed, we have fabricated a microcavity, in order to detect changes of the resonance wavelength consequent to changes of the refractive index of the gas. The resonant wavelength has been monitored measuring the reflectivity, which is close to 100% over the whole stop-band except at the resonance. Fig. 8 shows the response of both the resonance position and the current to changes in

humidity and in  $\text{NO}_2$  independently. We can appreciate that humidity quenches the electrical signal and red-shifts the reflectance peak. However,  $\text{NO}_2$  only leads to electrical response, as we do not observe any peak-shift. This fact allows us to conclude that, since the resonance shifts can be only associated to the presence of water vapor, a calibration of the

of positive carriers (holes) at the Si-electrolyte interface. Si dissolution occurs preferentially at the pore tips. However, if the hole supply is large, significant hole currents can be injected to the pore wall regions, causing pore widening during the anodization. In n-type Si, the growth of pores of very large aspect ratios can be achieved by limiting the hole supply from

electrical response for different humidity values would allow to calculate the  $\text{NO}_2$  concentration under any condition of humidity.

**5. Macroporous Si as a photonic crystal** The rationale behind the use of photonic crystals (PC) in optoelectronic devices can be found elsewhere [37]. Si is a good candidate to develop PC and here we review the production of two-dimensional 2D photonic crystals in Si by anodic electrochemical dissolution. Electrochemical dissolution process has many advantages with respect to other dry methods: it is simpler, cheaper, faster, technologically friendly, and wafer scalable.

The typical 2D PC that can be obtained with PS are constituted by air columns in a Si matrix. The air columns are the macropores, which are formed in Si when particular etching parameters are used. The formation of macropores in Si by anodic dissolution is a process optimized in the first years of ninety [38] and could be used to produce both pores and pillars lattices. In one of the most accepted (although not complete) model, the anodic dissolution of Si is assumed to occur because of the presence

the substrate. In p-type Si, however, hole density is set by the doping and cannot be easily controlled in the wall regions.

Thus, due to lateral dissolution, only limited aspect ratios are achievable.

Photonic crystals in p-type Si, on the other hand, are desirable for a number of reasons. First, the experimental setup does not require a light source to the backside of the wafer to generate holes as with n-type Si. Second, the obtained macroporous Si could be easily further used as substrate for nanoporous silicon, whose formation also requires hole injection and is best achieved in p-type Si. Third, p-type substrates are largely preferred for CMOS processes, suggesting easier integration potentiality with conventional electronics.

To form 2D PC, one has to control the macropore surface arrangement. To periodically order the macropores on the surface, an initial lithographic step transfers to the surface the initial etch pits pattern [39]. An attack in KOH, develops the etch pits. Subsequently these etch pits are deepened with the electrochemical dissolution. We have seen that addition of DMF or DMSO to the HF solution accelerates the

etching rates of the pore growth and shrinks the space charge regions. The combination of these two effects allows an high anisotropy of the dissolution process (Figure 9). The structures are very regular with a maximum aspect ratio of about 40.

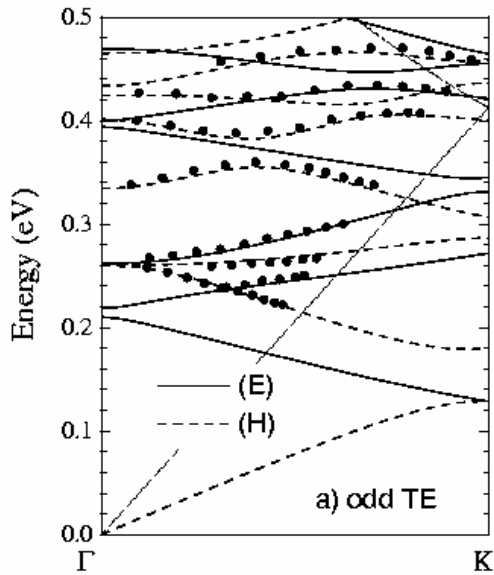


Figure 10. Points: measured dispersion of the photonic bands derived from structures in reflectance spectra; solid and dashed lines: photonic bands separated according to parity with respect to plane of incidence. TE-polarization, odd modes. The dispersion of free photons is indicated by dotted lines.

To test the photonic properties of the obtained structures, variable-angle reflectance measurements from the sample surface have been performed [40]. Figure 10 shows the results for a sample etched in DMF. Results are given for TE- and TM-polarized light incident along the  $\Gamma$ -K orientation. The angular dependent reflectance is characterized by prominent step-like features that display a well-defined dispersion as a function of the incidence angle  $\theta$ . These are associated with the excitation of photonic modes in the photonic crystal and may be regarded as “absorption” processes that give rise to spectral line-shapes similar to that of 1D critical points in semiconductors. From the experimental reflectance spectra, the dispersion of the photonic bands in a given direction can be extracted by plotting the energy positions of the observed step-like features versus the par-

allel wavevector. This analysis is reported in Figure 10, where the measured dispersion of photonic bands for TE-polarization (odd modes) is shown together with the calculated ones for the  $\Gamma$ -K direction. For the calculations the parameters of the photonic crystal extracted from SEM analysis have been used. The remarkable agreement between the experimental points and calculated bands of the proper parity as well as the observation of peculiar features typical of the photonic band structure, i.e. anticrossing between bands of the same symmetry, clearly demonstrate the high quality of these p-type macroporous silicon photonic crystals.

**6. Porous Si Fibonacci quasicrystals** Anderson localization is a wave phenomenon that can be described as an interference effect between counter propagating waves. If the amount of disorder is strong enough, a breakdown occurs in the diffusive wave transport, the diffusion constant vanishes and the waves become localized. A similar picture holds for light propagation in one-dimensional aperiodic structures [41-43]. Deterministic aperiodic structures are obtained by the iteration of some deterministic prescription, called the generating rule, but are characterized by the lack of any translational periodicity. A class of deterministic aperiodic structures is represented by the Fibonacci quasicrystals [44-46]: multilayers structures constructed recursively as  $S_{j+1}=\{S_{j-1}S_j\}$  for  $j \geq 1$ , where  $S_0=\{B\}$  and  $S_1=\{A\}$ . In this sequence,  $S_2=\{BA\}$ ,  $S_3=\{ABA\}$ ,  $S_4=\{BAABA\}$ ,  $S_5=\{ABABAAB A\}$ , and so on. Of particular interest is the possibility to address experimentally the question of light transport and localization in deterministic aperiodic structures, where the diffusion characteristics are strongly affected by the aperiodicity of the system on one side, and by the structure irregularities and random unavoidable perturbations on the other side.

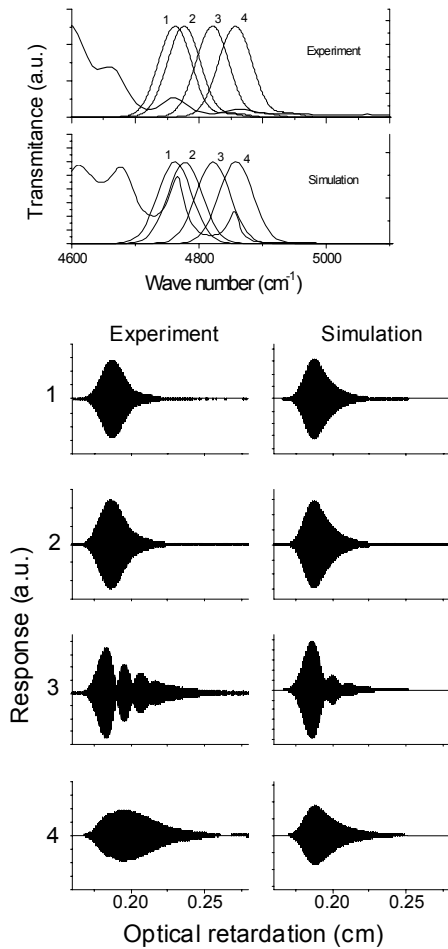


Figure 11. Upper plots: measured band-edge and input laser profiles ('Experiment'), simulations of the sample band-edge with the incident gaussian laser pulses ('Simulation'). Lower plots: measured ('Experiment') and simulated ('Simulation') time response of the sample corresponding to the different pulses indicated by the numbers in the figure.

Here we report the band edge pulse propagation of PS Fibonacci quasicrystals, where the most dramatic effects are expected. To address this question, we have grown electrochemically a Fibonacci quasicrystal with  $j=12$  (up to 233 layers) starting from a  $p^+$ -type doped Si wafer.  $S_0$  was a 165 nm thick layer with 66% of porosity and  $S_1$  was a 110nm thick layer with 45% of porosity. The total thickness of the 233 layers sample was approximately 30 $\mu$ m. The band-edge transmission spectrum of the Fibonacci structure was simulated by a transfer matrix method [47]. To obtain a good agreement with the experiments, the simulation

included a small linear drift both in the layer thickness and porosities. Taking into account these corrections it is possible to obtain a good agreement with the measured transmission spectrum of the structure only in the frequency region below 5500 $\text{cm}^{-1}$ , where the absorption of the Si substrate and of PS itself is negligible. We focused our attention only in a narrow region of about 500  $\text{cm}^{-1}$  at the band edge, where the time dynamic of femtosecond laser pulses transmitted through the Fibonacci samples and spanning in frequencies the entire band edge have been studied by means of phase sensitive interferometric techniques [48]. In Fig. 11 we show some of the input gaussian laser pulses that are in resonance with the band-edge, together with the measured and calculated time response of the structure. The transmitted pulse lineshapes depend on the energy of the pulses. When the pulse energy is resonant with only a single optical mode (single transmission peak in Fig. 11 top), the pulse is significantly delayed and exponentially stretched (e. g. Fig. 11 curve 4). In addition to the delay and stretching, when the pulse energy overlaps two narrow transmission modes (e. g. Fig. 11 curve 3) a coherent beating between these different modes is observed whose oscillation frequency corresponds to the frequency difference between the excited optical modes.

The pulse delay is due to both the band-gap effect and to the localized character of the band-edge mode that has been excited. It is well known [49] that even in perfectly ordered and periodic structures localized modes, called band-edge resonances, can appear at the band-edge. These modes are extremely narrow and are characterized by an enhancement of the electromagnetic field. The field enhancement is due to the interplay of a quasi-standing wave, transiently formed inside the layered structure, and the forward propagating electromagnetic field of the propagating pulse. Within this simplified physical picture, energy is scattered from the forward propagating fields into the quasi-standing wave, and back into the forward propagating fields. The wave oscillates inside the crystal and can transiently store a substantial amount of the electromagnetic energy. This effect is manifested in our experiment by the large stretching of the pulse.

The resonant excitation of two adjacent narrow transmission modes produces the observed coherent beating in the time domain. For incident pulses far away from the band-edge no such effects have been measured.

**7. Conclusions** Initiated by technical investigations in the 1940s, and started as an industry in late 60s, the planar Si technology has distinguished itself by the rapid improvements in its products. While the indirect nature of its band-gap on one hand, and the satisfactory performance of CMOS electronic devices on the other have postponed any significant investment in Si photonics up to the nineties, we believe now that the perspective on Si photonics is no more unrealistic. On the material side, the rapidly growing nanotechnology has shown that the optical properties of bulk crystalline materials can be dramatically changed by shrinking their sizes. On the application side, we have witnessed a number of intriguing discoveries in the interaction between light and matter, such as quasicrystals and photonic band-gaps. Simultaneously, the integration level and interconnect bandwidth requirements are pushing harder towards the introduction of optical functionality inside integrated circuits.

In the last decade Si LEDs and optoelectronic devices, optical gain in Si nanocrystals and Si photonic band-gap materials have been demonstrated. A lot of such achievements have been first observed in nanoporous or in macroporous Si, whose fabrication procedure is very inexpensive. At present PS is difficult to control, in particular with respect to its growth and its stability in time. It is hard to predict whether it will be possible to control the stability to the degree required by the applications. Even though it might be necessary to employ different – and certainly more expensive – procedures for Si-nc fabrication, the availability of PS has been a fortunate circumstance to widely demonstrate feasibility of Si-based photonics. The race is now open to reach a fully all-Si based integrated photonic circuit.

**Acknowledgements** The work here reported is the outcomes of numerous collaborations. On Si-nc with INFM of Catania and Modena and with IMM-Catania of CNR. It has been carried

out in the framework of the special project LUNA and the advanced research project RAMSES of INFM. It has been also supported by MURST through the program COFIN99. On PC with the Microsystem Division of ITC-irst, and University of Pavia. It was supported by MURST through the program COFIN00. On Fibonacci quasicrystals with the Van der Waals – Zeeman Institute of Amsterdam and L.E.N.S. in Florence. It has been supported by the University of Trento through the program Giovani Ricercatori M.A.R.C. and by INFM through the project RANDLAS. On PS sensor with INFM of Brescia and financed by INFM through the project SMOG and by PAT. Among the others we thank S. Ossicini for fruitful discussion and theoretical support.

#### Reference:

- [1] International Technology Roadmap for Semiconductors, 2000 Update, Interconnect (electronic document at <http://public.itrs.net>.)
- [2] *Silicon based microphotonics: from basics to applications* 1999 edited by Bisi O, Campisano S U, Pavesi L and Priolo F (Amsterdam: IOS press)
- [3] Gelloz B and Koshida N 2000 *J. Appl. Phys.* **88** 4319
- [4] Green M. A., Zhao J., Wang A., Reece P. J. and Gal M. 2001 *Nature* **412** 805
- [5] Pavesi L, Dal Negro L, Mazzoleni C, Franzò G and Priolo F 2000 *Nature* **408** 440
- [6] Bisi O, Ossicini S and Pavesi L 2000 *Surf. Sci. Rep.* **264** 1
- [7] Lettieri S, Maddalena P, Odierna L P, Ninno D, La Ferrara V, Di Francia G 2001 *Phil. Mag (B)*. **81** 133
- [8] Vijaya Lakshmi S, Shen F and Grebel H 1997 *Appl. Phys. Lett.* **71** 3332
- [9] Vijaya Lakshmi S, George M A, Grebel H 1997 *Appl. Phys. Lett.* **70** 708
- [10] Borsella E, et al. L 2001 *Mat. Scie., Eng.* **B79** 55
- [11] Vijaya Prakash G, Cazzanelli M, Gaborro Z, Pavesi L, Iacona, F, Franzò G and Priolo F 2002 *J. Mod. Optics* **49** 719
- [12] Sheik- Bahae M, Said A A and Van Stryland E W 1989 *Opt. Lett.* **14** 955
- [13] Vogel E M, Weber M J, and Krol D M 1991 *Phys. Chem. Glasses* **32** 231
- [14] Reitze D H, Zang T R, Wood W M and Downer M C 2000 *J. Opt. Soc. Am.* **B 7** 84

- [15] Lettieri S, Fiore O, Maddalena P, Ninno D, Di Francia G and La Ferrara V 1999 *Opt. Commun.* **168** 383
- [16] Schmitt-Rink S, Miller D A B and Chemla D S 1987 *Phys. Rev. B* **35** 8113
- [17] Hanamura E 1988 *Phys.Rev.B* **37** 1273
- [18] Vijaya Prakash G, et al. 2001 *J.Nano Sci. Nano Tech.* **1** 159
- [19] Klimov V.I., et al. 2000 *Science* **290** 314, 2000
- [20] Khriachtchev L., Rasanen M., Novikov S., Sinkkonen J., 2001 *Appl. Phys.Lett.* **79** 1249
- [21] Nayfeh M.H., et al., 2002 *Appl.Phys.Lett.* **80** 121
- [22] Luterová K., et al., 2002 *Appl. Phys. Lett.*, **91** 2896
- [23] Shaklee K L, Nahaory R E and Leheny R F 1973 *J. Lumin.* **7** 284
- [24] Zhou F., Head J.D., 2000 *J.Phys.Chem.B* **104** 9981
- [25] Puzder A., Williamson A.J., Grossman J.C., Galli G., 2002 *Phys.Rev.Lett.*, **88** 97401
- [26] Filonov A.B., Ossicini S., Bassani F., Arnaud d'Avitaya F., 2002 *Phys. Rev. B*, **65** 195717
- [27] Baierle R.J., Caldas M.J., Molinari E., Ossicini S 1997 *Solid State Communications*, **102** 545
- [28] Yu Kobitski A., Zhuravlev K.S., Wagner H.P., Zahn D.R.T., 2001 *Phys.Rev. B.* **63** 115423
- [29] Mulloni V and Pavesi L 2000 *Appl. Phys. Lett.* **76** 2523
- [30] Harper J and Sailor M J 1996 *Anal. Chem.* **68** 3713
- [31] Baratto C, Faglia G, Sberveglieri G, Boarino L, Rossi A M and Amato G 2001 *Thin Solid Films* **391** 261
- [32] Mares J J, Kristofik J and Hulicius E 1995 *Thin Solid Films* **255** 272
- [33] Foucaran A, Sorli B, Garcia M, Pascal-Delannoy F, Giani A and Boyer A 2000 *Sens. Act. A* **79** 189
- [34] Gaburro Z, Daldosso N, Pavesi L, Faglia G, Baratto C and Sberveglieri G 2001 *Appl. Phys. Lett.* **78** 3744
- [35] Chan S, Fauchet P M, Li Y, Rothberg L J and Miller B L 2000 *Phys. Stat. Sol. A* **182** 541
- [36] Pavesi L 1997 *La Rivista del Nuovo Cimento* **20** 1
- [37] Weisbuch C, Benisty H, Olivier S, Rattier M, Smith C J M and Krauss T F 2000 *Phys. Stat. Sol. (b)* **221** 93
- [38] Lehmann V and Föll H 1990 *J. Electrochem. Soc.* **137** 653; Lehmann V and Rönnebeck S 1999 *J. Electrochem. Soc.* **146** 2968
- [39] Schilling J., et al. 2001 *J. Opt A:Pure Appl. Opt.* **3** S121.
- [40] Galli M., et al., 2002 *Phys. Rev. B* **65** 113111
- [41] Gellermann W, Kohmoto M, Sutherland B and Taylor P C 1994 *Phys. Rev. Lett.* **72** 633
- [42] Kohmoto M, Sutherland B and Iguchi K 1987 *Phys. Rev. Lett.* **58** 2436
- [43] Peng R W, Wang M, Hu A, Jiang S S, Gin G J and Feng D 1998 *Phys. Rev. B* **57** 1544
- [44] Kohmoto M and Sutherland B 1987 *Phys. Rev. B* **35** 1020
- [45] Desideri J P, Macon L and Sornette D 1989 *Phys. Rev. Lett.* **63** 390
- [46] Capaz R B, Koiller B and Queiroz S L A 1990 *Phys. Rev. B* **42** 6402
- [47] F.L. Pedrotti, L.S. Pedrotti, *Introduction to Optics*, Prentice-Hall, (1987)
- [48] Imhof A., Vos W.L., Sprik R., Lagendijk A., 1999 *Phys. Rev. Lett.* **83**, 15, 2942 (1999); Kop Rik H.J., Sprik R., 1995 *Rev. Sci. Instrum.* **66** 5459
- [49] Scalora M, Flynn R J, Reinhardt S B, Fork R L, Bloemer M J, Tocci M D, Bowden C M, Ledbetter H S, Bendickson J M, Dowling J P and Leavitt R P 1996 *Phys. Rev. E* **54** 1078